



OPEN PEGDA-based HistoBrick for increasing throughput of cryosectioning and immunohistochemistry in organoid and small tissue studies

Emilie Vuille-dit-Bille^{1,2,5}✉, Larissa Utz^{3,4,5}, Fiona E. Müllner^{3,4}, Valeria J. Arteaga-Moreta^{3,4}, Yanyan Hou^{3,4}, Stefan E. Spirig^{3,4}, Diane Ledroit-Paic¹, Sarah Heub¹, Jonas Goldowsky¹, Gilles Weder^{1,6} & Magdalena Renner^{3,4,6}✉

Histology is the gold standard for analyzing tissue structure and cell morphology. Immunostaining on thin tissue sections enables precise visualization of antigens and proteins. However, for cryosectioning small tissues such as organoids, spheroids, and tumoroids there is a lack of standardized, time- and cost-effective methods, limiting the throughput of analysis. Here, we have adapted to cryosectioning our previously developed HistoBrick approach, in which small tissue arrangement is spatially controlled within arrayed mini-wells. By testing various embedding matrices, we show that an 8% PEGDA and 2.5% gelatine mixture is optimal, providing essential structural support to maintain sample integrity during cryosectioning. This embedding matrix preserves fragile substructures of human retinal organoids, which are particularly susceptible to damage during sample preparation. Using PEGDA-gelatine HistoBricks for the simultaneous embedding of 16 retinal organoids, we analyzed a time course of retinal organoid development. We observed the maintenance of photoreceptors cell bodies up to week 98 in culture, while photoreceptor outer segments were gradually lost. Further, we observed displaced photoreceptors in the region of outer segments. The PEGDA-gelatine HistoBrick is a cost-efficient tool that can be implemented for small tissue studies to increase throughput in experiments such as large-scale screenings or toxicology research.

Keywords 3D cell models, Microtissues, Organoids, Spheroids, Human retinal organoids, Histology, Cryosection, HistoBrick

Histology provides insights into tissue structure and cellular morphology and is the gold standard analytical method for clinicians and researchers. Tissue sectioning along with immunohistochemical staining reveals changes in tissue morphology or physiology in response to different treatments and environments. Histological sections are most commonly prepared via paraffin infiltration or cryosectioning. In terms of antigen accessibility for immunohistochemical stainings, cryosections are considered to be superior to paraffin sections. Paraffin infiltration hides some of the antigens, necessitating long non-standardized antigen retrieval protocols for immunostaining. Cryosectioning generally preserves antigens well and enables their visualization via immunohistochemistry^{1,2}.

Microtissues (organoids, spheroids, tumoroids and related complex 3D cellular models) serve as invaluable *in vitro* models of tissues, offering insights into organ development, disease phenotypes and drug responses^{3,4}. While some microtissues can be produced in large numbers, their high-throughput analysis remains a challenge⁵⁻⁷. Preparing histological sections to analyze microtissues or small tissues is a low-throughput, labor-intensive and operator-dependent process^{8,9}. Typically, the operator manually embeds a few (less than ten) microtissues into

¹CSEM SA, Neuchâtel, Switzerland. ²Institute of Mechanical Engineering, EPFL, Lausanne, Switzerland. ³Institute of Molecular and Clinical Ophthalmology Basel, Basel, Switzerland. ⁴Department of Ophthalmology, University of Basel, Basel, Switzerland. ⁵Emilie Vuille-dit-Bille and Larissa Utz have contributed equally to this work. ⁶Gilles Weder and Magdalena Renner have share the senior authorship. ✉email: emilie.vuille-dit-bille@csem.ch; magdalena.renner@iob.ch

a matrix to form a block (Fig. 1a). Because individual microtissues in the block cannot be easily traced during conventional embedding and subsequent analysis steps, often one or multiple blocks need to be prepared per experimental condition. The time-consuming histological process is especially a bottleneck in the field of drug discovery, where large numbers of compounds are often validated in multiple sample replicates⁷.

Strategies have been deployed to increase the throughput of microtissue histology. We and others have described planar arrays to spatially organize samples within blocks^{8–14} or to centrifuge samples for arrangement on the same sectioning plane¹⁵. For cryosectioning, tissue microarray-inspired approaches remain limited either in terms of alignment precision, intensive labor, or process compatibility with various microtissue culture approaches^{9,14}. An ideal and versatile method to increase throughput of microtissues histological analysis should provide: 1. Spatially organizing microtissues in the sectioning plane to trace individual samples throughout the entire study, allowing the combination of different experimental conditions within one block; 2. Highly increasing the number of microtissues within one block; 3. Aligning microtissues in a narrow horizontal plane in the embedded block to reduce the number of sections required for the analysis; 4. Ease-of-use and standardized procedure involving readily accessible tools and materials with integration potential in automated workflows.

We aimed to create a solution adapted to cryosectioning that addresses the previous advantages by improving our previously established HistoBrick tool, in which spheroid arrangement is spatially controlled in a paraffin embedded agarose block with arrayed mini-wells⁸ (Fig. 1b). Because the original agarose-based HistoBrick is not suited for cryosectioning, there is a need to develop a HistoBrick made of a cryosectioning-compatible material. The selection of a suitable embedding matrix for HistoBrick preparation is crucial to ensure the integrity of the frozen block (also called cryoblock) throughout the sectioning process. Fragile samples that lack rigidity (neuronal tissue), contain cavities (cochlea biopsy), or present complex surface topography (retinal organoids) can be structurally distorted during cryosectioning, rendering analysis of their immunostaining less informative^{16–18}. Optimal Cutting Temperature compound (OCT) is a widely used matrix for embedding samples for cryosectioning. However, OCT melts at room temperature, leaving the histological sections which may disrupt fragile sample structures¹⁹. Gelatine is preferred by some scientists to embed soft tissues such as brain and cochlea. One advantage of gelatine is the mechanically stable sample-matrix interfaces^{16,17,20}. However, gelatine presents the disadvantage of needing to be kept above 37 °C to stay liquid. At room temperature, the viscosity of gelatine increases, making pipetting difficult. Other hydrogels, such as PEGDA, have a stable viscosity at room temperature and their crosslinking can be precisely controlled using UV light. However, PEG-derived hydrogels alone are not suitable for cryosectioning²¹.

Here, we describe a new hydrogel mixture composed of PEGDA, gelatine and sucrose suited for HistoBrick preparation and cryosectioning. The new material composition is tested against different parameters including ease of preparation, integrity of cryosections, vertical alignment of microtissues and preservation of their structure. The impact of the embedding matrix on the structural integrity of the sample is studied using retinal organoids. Retinal organoids, like the adult human retina, are organized in layers containing different cell types^{22,23}. Along the outer organoid surface, they present particularly fragile, hair-like structures made

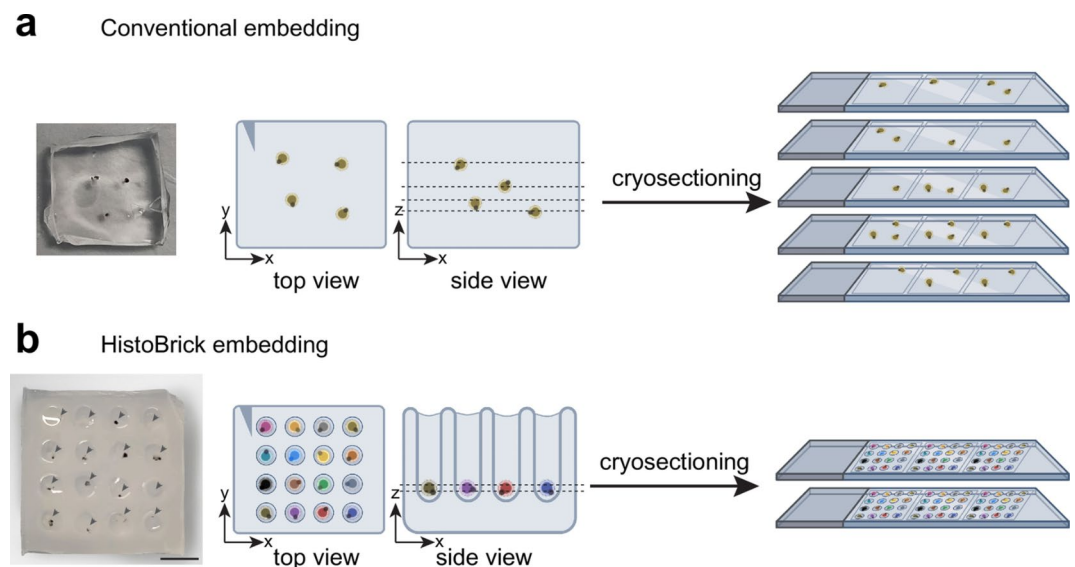


Fig. 1. Illustration of conventional and HistoBrick embedding. **(a)** Photograph of a conventionally embedded block (left) and schematic illustration of a block with conventional embedding of multiple retinal organoids from one experimental condition (middle). Resulting organoid distribution in the different slides prepared during cryosectioning (right). **(b)** Photograph of a HistoBrick with arrowheads pointing to white organoids, while some organoids contain pigmented retinal pigment epithelium cells appearing black on the photograph (left, scale bar: 5 mm). Schematic illustration of a HistoBrick filled with 16 retinal organoids of different experimental conditions (middle). Resulting organization of the slides obtained after cryosectioning (right).

of light-sensitive photoreceptor outer segments. Cells of the human retina, in particular photoreceptors and their outer segments, are affected by several diseases leading to blindness^{24,25}. Reliable visualization of retinal layers, photoreceptors and their outer segment structures is thus essential. We confirm that the new embedding material for cryosectioning preserves layering of the organoids, photoreceptor appearance and the fragile outer segments throughout the histological process.

Taking advantage of PEGDA-gelatine HistoBricks, we analyze a two-year time-course of retinal organoid development and describe features of human retina degeneration (such as the loss of photoreceptor outer segments) and features of human retina aging (such as displaced photoreceptors in the region of outer segments). Embedding up to 16 retinal organoids from different experimental conditions into one HistoBrick increases the throughput of microtissue histological analysis for cryosectioning, while decreasing cost of the analysis by saving reagents and time.

Results

Optimizing hydrogel formulation for HistoBrick preparation and cryosectioning

We aimed to identify a hydrogel to adapt the HistoBrick method to cryosectioning. The HistoBrick was prepared by first filling liquid embedding material into a silicone mold, and subsequently crosslinking to obtain a gel well plate. The gel well plate contained an array of mini-wells in which microtissues were transferred. After sedimentation of the microtissues to the well bottom, the wells were filled by liquid embedding material and the resulting HistoBrick was snap frozen and cut into thin Sections (10–30 μm) on a cryostat (Fig. 2). In this manuscript, the word HistoBrick refers to both the embedding method and the resulting block containing the gel well plate, the microtissues and the embedding matrix. The gel well plate is the empty arrayed hydrogel and the embedding matrix is the hydrogel in direct contact with the microtissues in the wells. The gel well plate and the embedding matrix are always made of the same material. After snap freezing, the frozen HistoBrick is called cryoblock.

We first tested the fabrication and cryosectioning of the HistoBrick with either gelatine or PEGDA, not containing microtissues. OCT was not considered for HistoBrick fabrication because an OCT HistoBrick would need to be loaded while frozen which would not allow sedimentation of small samples that would freeze along the cold wells at random heights. We successfully molded gel well plates with the two materials. While crosslinking of the gel well plate prepared with gelatine required one hour at 4 $^{\circ}\text{C}$, crosslinking with UV for the PEGDA solution only took a few minutes. The unmolding of the gelatine gel well plate was more challenging than the one prepared of PEGDA, as solidified gelatine tended to stick to the silicone mold. We subsequently investigated the integrity of the sections, and the interface between the gel well plate and the embedding matrix. Sectioning the PEGDA HistoBrick (8 v% and 10 v% PEGDA) resulted in frequent wrinkling and breakage of the sections, highlighting poor mechanical stability. Additionally, filling the PEGDA gel well plate with PEGDA solution resulted in a non-adherent interface, which led to the disassociation of the embedded matrix from the gel well plate (Fig. 3a left). Consequently, some embedding matrix regions were lost or folded during sectioning. During an analysis experiment containing organoids this would result in the loss of microtissues located inside. The sections of the gelatine HistoBricks were stable without major cracks or folds, and with good cohesion at the interface of the well plate and embedding matrix (Fig. 3a middle). Due to its poor sectionability, the PEGDA hydrogel was not used for further testing with organoids.

To promote a coherent interface between organoids and the embedding matrix, organoids were incubated in the embedding solutions for 15 min prior to the transfer into the gel well plate. The pipetting of organoids, incubated in gelatine solution, into the wells trapped air bubbles at the bottom. The presence of air bubbles at the bottom of the wells prevented the organoids from sedimenting and aligning on a unique plane while reducing the integrity of the sections during cutting. An additional barrier to a planar arrangement of organoids

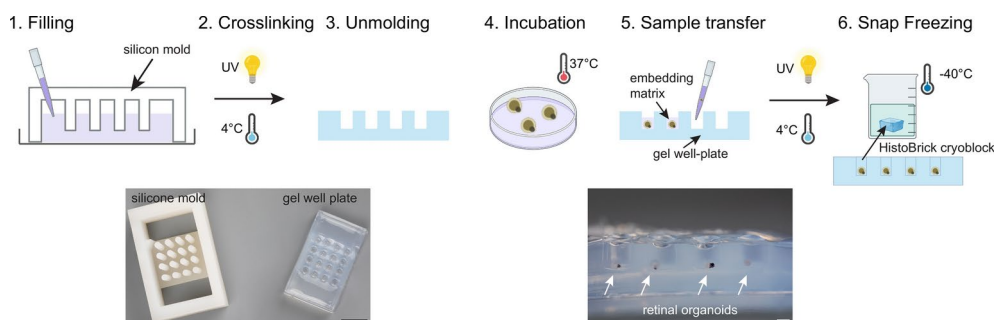


Fig. 2. Schematic of HistoBrick cryoblock fabrication steps. 1. The silicone mold is filled with the liquid hydrogel solution; 2. The hydrogel solution is crosslinked either by UV or at 4 $^{\circ}\text{C}$ for PEGDA and gelatine respectively; 3. The gel well plate is unmolded; 4. The retinal organoids are incubated in the embedding matrix (same hydrogel solution as for the fabrication of the gel well plate) at 37 $^{\circ}\text{C}$; 5. The organoids are transferred with the embedding matrix into the gel well plate, sedimented to the bottom of the plate, followed by crosslinking; 6. Snap freezing. Photograph of the silicone mold and gel well plate (bottom left, scale bar: 10 mm). HistoBrick containing the gel well plate, organoids and embedding matrix (bottom right, scale bar: 1 mm).

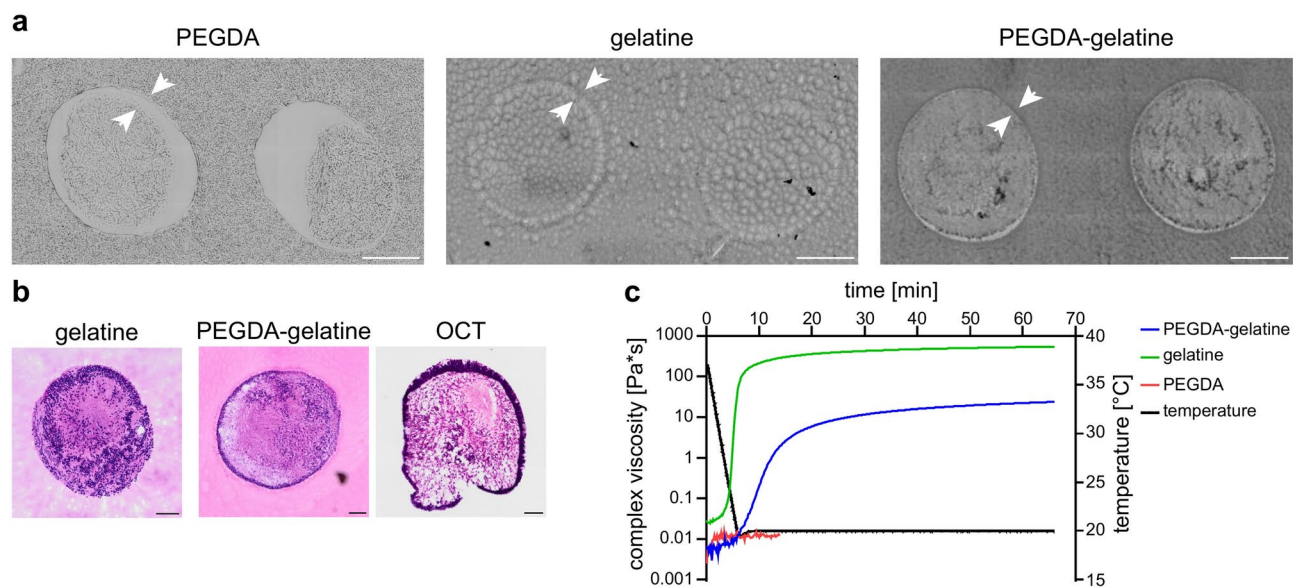


Fig. 3. Comparison of different embedding materials on cryosectioning and rheological properties. **(a)** Brightfield images of the HistoBrick cryosections (of 20 μm thickness) made of PEGDA (8%), gelatine (7.5%) and PEGDA-gelatine (8% PEGDA and 2.5% gelatine) solution, showing the interface (arrowheads) between the HistoBrick well plate and the embedding matrix. No microtissues were embedded in the HistoBricks and thus no organoids are present in the sections. (scale bar: 1 mm). **(b)** H&E staining of retinal organoids (all organoids were fixed in week 33, $n = 4$ organoids for each embedding) showing the interface of the embedding matrix and organoids. For gelatine HistoBrick embedding, PEGDA-gelatine HistoBrick embedding, and OCT conventional embedding, sections are of 20 μm thickness (scale bar: 100 μm). **(c)** Complex viscosity in function of time with a temperature profile going from 37 to 20 $^{\circ}\text{C}$ and stabilizing.

in gelatine HistoBricks was their tendency to attach to the sides of the wells during transfer. Consequently, we had to gently push them down to the bottom of the wells using a pipette tip.

To optimize organoid planar embedding and HistoBrick sectioning, we aimed to build on the advantages of both tested materials. We developed a new embedding matrix by mixing 8 v% PEGDA with 2.5 wt% of gelatine (thereafter called PEGDA-gelatine hydrogel). The PEGDA-gelatine HistoBrick combined the fast and easy unmolding of the PEGDA HistoBrick and the structural stability and coherence of embedding matrix-gel well plate interface during cryosectioning of the gelatine HistoBrick (Fig. 3a right). We did not observe air bubble trapping when pipetting organoids incubated in PEGDA-gelatine solution and organoids efficiently sedimented to the bottom of the wells.

We then investigated the interface between the organoids and the embedding matrix in more detail with a hematoxylin and eosin staining, as a coherent interface is important to support the tissue structure. Eosin stained the proteins contained in gelatine and thus enabled embedding matrix visualization. Both gelatine and PEGDA-gelatine matrix presented a stable interface with the organoids, meaning that the embedding matrices did not detach from the organoid surface throughout the whole histological process (Fig. 3b). The gelatine sections have a structure less homogeneous than the PEGDA-gelatine sections but this was not found to impact the interface with the organoids. Conventional embedding in OCT was also performed, as it is known to present a weak interface¹⁹. Indeed, during the staining procedure the OCT was washed away, not maintaining an interface with the tissue (Fig. 3b).

Hydrogel rheological analysis

We next aimed to understand how viscosity of the hydrogel solutions affected their compatibility with organoid transfer procedures. Using rheology, we measured changes in viscosity of the PEGDA, gelatine, and PEGDA-gelatine solutions over time at temperatures representative of the HistoBrick loading step. To recreate similar conditions, the measurements were started with a temperature ramp going from 37 to 20 $^{\circ}\text{C}$ (5 $^{\circ}\text{C}/\text{min}$), followed by an isotherm at 20 $^{\circ}\text{C}$ (Fig. 3c). As the solutions underwent temperature-driven crosslinking during the tests, we measured the complex viscosity that considered the elastic and viscous component of crosslinked hydrogels. The complex viscosity of the PEGDA solution stayed stable throughout the whole experiment. The isotherm at 20 $^{\circ}\text{C}$ was shortened as the PEGDA solution showed a stable behavior. The viscosity of the gelatine solution started to increase during the temperature ramp at 22 $^{\circ}\text{C}$ and stabilized at the end of the ramp when the temperature reached 20 $^{\circ}\text{C}$. The increase of viscosity was caused by the crosslinking of the gelatine polymers inside the solution upon cooling. On the other hand, the viscosity of the PEGDA-gelatine solution started to increase at 20 $^{\circ}\text{C}$ and stabilized 6 min later. The PEGDA polymers do not influence the viscosity as in these experiments no UV crosslinking was performed. Therefore, the difference between the two solutions is interpreted to come from the difference in gelatine concentration. These results support experimental observations that PEGDA-gelatine

solution was easier to handle when pipetting into the gel well plate due to its slower increase of viscosity during the process.

PEGDA-gelatine preserves fragile organoid substructures

To investigate if the embedding process of the HistoBrick has an impact on the structure of fragile organoid substructures, we used human retinal organoids. Like the human retina, retinal organoids are structured into layers with each layer containing specific cell types. Photoreceptor cell bodies are arranged in a layer called outer nuclear layer along the outside of retinal organoids. The inner nuclear layer and ganglion cell layers of retinal organoids, like the human adult retina, contain the other major cell types of the neural retina as described in Cowan et al.²² (Fig. 4a). Along the outer surface, retinal organoids display fragile outer segments. Outer segments are the light-sensitive “antennae” of photoreceptor cells. We embedded PFA-fixed, outer-segment-containing retinal organoids from the same organoid differentiation and compared conventionally embedded to HistoBrick embedded samples using both gelatine and PEGDA-gelatine as embedding materials. We evaluated both, overall organoid integrity, and the maintenance of outer segments on cryosections (Fig. 4, Supplementary Fig. 2). As a negative control, we embedded retinal organoids in OCT, as we and others have described that this treatment does not preserve outer segments^{18,22}. Due to the liquid state of OCT at room temperature and its very high viscosity, we used it only for conventional embedding.

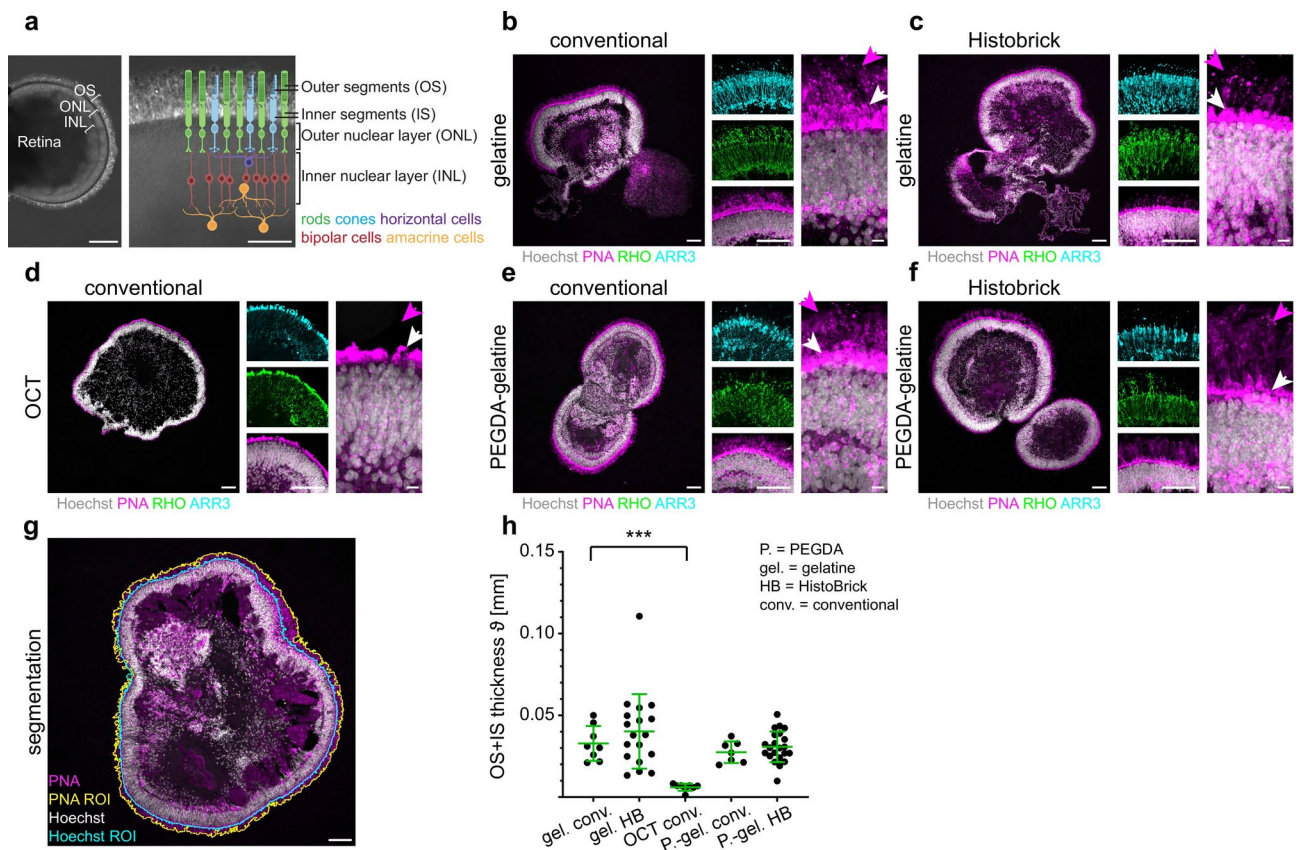


Fig. 4. Investigation of the influence of the different embedding materials on human retinal organoids and their sensitive outer segments. **(a)** Phase contrast live image of a representative retinal organoid (scale bar: 200 μm) and a schematic illustration of retina layers and different cell types and a phase contrast live image of a mature organoid in the background (scale bar: 50 μm). **(b–f)** Immunohistochemistry staining of embedded organoids using different embedding methods and materials to validate organoid preservation during embedding. The pink arrowheads indicate the stained outer segments, while the white arrowheads point to the inner segments. The sections are 25 μm thick. The overview images of whole organoids are of one Z plane (scale bar: 100 μm), higher magnification images of a part of the retina are maximum Z projections of Z stacks (scale bar: 100 μm for the images in the middle of each subfigure; and 10 μm for the images on the right of each subfigure) **(g)** Example image of organoid with segmented OS + IS (yellow segmentation line) and organoid area (cyan segmentation line) (scale bar: 100 μm). **(h)** Quantification of OS + IS thickness ϑ of retinal organoids. The organoids of Fig. 4b–f were quantified, and each dot represents an individual organoid. All organoids ($n = 63$ organoids) were from one differentiation experiment, fixed at week 35, and distributed to the different embedding conditions for analysis. Mean \pm SD shown in green. One-way Welch’s ANOVA, P value < 0.001 ; posthoc Dunnett’s test comparing gelatine conventional to all other groups, ***adjusted P value < 0.001 . Only significant P value indicated in the graph, all other comparisons were not significant.

To analyze retinal organoid sections obtained using the different embedding materials we performed immunostainings (Fig. 4b–f). For visualization of cone photoreceptors, we stained them with an antibody against arrestin 3. Rod photoreceptor morphology was visualized using an antibody against rhodopsin labelling rod cell bodies in the outer nuclear layer and rod outer segments as thin appendices and dots surrounding the organoid. For both conventional and HistoBrick embedding using gelatine and PEGDA-gelatine, and for OCT embedding, the outer nuclear layer containing cone (ARR3 positive) and rod (RHO positive) photoreceptor cell bodies was well preserved (Fig. 4b–f). We stained for various retinal cell types, like cones expressing M- and L-opsin, horizontal cells (ONCUT2 positive), ON bipolar cells (TRPM1 positive), Müller cells (RLBP1 positive), and ribbon synapses (Basson) and observed that organoid sections were well maintained and the cell types, as well as ribbon synapses, could be detected across all conditions (Supplementary Fig. 2a–e).

To observe cone outer segments, we stained organoid cryosections with the lectin Peanut agglutinin (PNA). PNA in retinal organoids labels both inner segments and outer segments of cones (Supplementary Fig. 2f). Cone inner segments appear bud-like adjacent to the outer nuclear layer, and the outer segments extend significantly farther than the inner segments (Supplementary Fig. 2f). In both gelatine and PEGDA-gelatine cryoblock preparations (conventional and HistoBrick embedding), RHO and PNA staining confirm the presence of cone and rod outer segments along the outside of retinal organoids (Fig. 4b–f). Upon OCT embedding, the RHO and PNA positive outersegments were completely lost, and only PNA-positive and RHO positive inner segment buds remained (Fig. 4d). Our stainings revealed that gelatine in some cases did not preserve outer segments well, leading to stretched outer segments, holes in the outer segment area that overall appeared rather porous, or outer segments ripped off the organoid (Supplementary Fig. 2g–i). While we observed those artefacts for both conventional and HistoBrick embedding using gelatine, it happened more frequently using the HistoBrick. Interestingly, we observed less damage to outer segments in the form of stretching or holes using PEGDA-gelatine than using gelatine embedding, irrespective of conventional or HistoBrick embedding. To quantify the preservation of outer segments, we estimated the average thickness ϑ of the PNA-positive outer and inner segments (“OS + IS thickness”) under different embedding conditions. We first defined a region-of-interest (ROI) of the retinal organoid by the PNA signal (PNA ROI), which contained outer segments, inner segments and the inner part of the retinal organoid. We then defined a ROI of the retinal organoid by the Hoechst signal (Hoechst ROI), which contained nuclei and the inner part of the retinal organoid but excluded outer and inner segments. The area of the outer and inner segments (OS + IS area) was estimated by subtracting the area of the Hoechst ROI (Hoechst area) from the area of the PNA ROI (PNA area; Fig. 4g and Supplementary Fig. 3b–e). The OS + IS thickness ϑ was estimated from the PNA area and the Hoechst area by a circular approximation (Methods) and was independent of the Hoechst area (Supplementary Figs. 3f, g and 5i, j), which varied due to variance in organoid size (Supplementary Fig. 3h,i) or cross-section area.

A significant reduction in ϑ was observed comparing samples conventionally embedded in OCT to the gelatine control. There were no significant differences in ϑ for organoids treated with conventional gelatine embedding compared to gelatine HistoBrick, conventional PEGDA-gelatine, or PEGDA-gelatine HistoBrick embedding, respectively. Overall, these results show that PEGDA-gelatine is suitable for HistoBrick preparation and well preserves organoid layering and fragile photoreceptor outer segments.

The HistoBrick improves organoid traceability and analysis throughput

We optimized the HistoBrick design to contain up to 16 retinal organoids while keeping external dimensions compatible with cryosectioning (Fig. 5a). Organoid diameters are on average 1.17 mm (+/- 0.25 mm SD; $n = 16,306$ organoid images quantified from²⁷ but can measure up to 2.66 mm (Supplementary Fig. 3i). We designed the HistoBrick wells to be 2.4 mm in diameter. Up to three sections of the HistoBrick fit on one glass slide. Here, we show an example with two sections enabling the simultaneous analysis of up to 32 organoids (Fig. 5b). Sometimes, the interface between the embedding matrix and the gel well plate is not continuous. Residual PBS, from the pre-wetting of the wells, is hypothesized to not be fully mixed with the embedding matrix, thereby disrupting the interface. Sedimentation of organoids at the bottom of the wells results in serial cryosections with maximized information content per section. More than 80% of organoids were present in the cryoblock over a thickness of $390 \pm 212 \mu\text{m}$, which corresponds to 19 ± 10 consecutive sections of $20 \mu\text{m}$. This large standard deviation is hypothesized to come from the heterogeneity of organoids size (Supplementary Fig. 3h,i) and morphology. In addition, the HistoBrick is often cut at a slightly tilted angle on the cryotome. A tilting angle between the HistoBrick and the blade was indicated by the fact that some wells only appeared in later sections (Supplementary Fig. 4a,b). Due to this misalignment, aligned organoids in the blocks would appear on different sections. The tilting angle inherent to manual sectioning was analyzed in more detail in our previous work and was hypothesized to reduce the number of visible organoids on the Sections⁸.

The individualization of organoids in an array facilitates their traceability throughout the analysis process from embedding into the HistoBrick to the sectioned samples on slides. When serial sections are prepared on consecutive glass slides, each organoids position can be tracked within the array. The different slides can be stained with various sets of dyes and antibodies, thus providing multiple datasets for a single organoid. First, the high information content obtained by immunohistochemistry on consecutive sections facilitates the correlation between the organoid structure and immunolocalization (Fig. 5b, c). Second, consecutive organoid sections can provide some insight into organoid 3D structure (Fig. 5b, d; Supplementary Fig. 4b). Finally, increasing the number of organoids embedded within one block makes their analysis cheaper. While in conventional blocks our lab previously embedded on average 4 organoids, the HistoBrick fits 16 organoids. Thus, depending on the scale of a performed experiment, using the HistoBrick can save 91% of sectioning time and 88% of reagents necessary for antibody stainings in an experiment in which 2 organoid replicates per treatment are analyzed (Supplementary Fig. 4d).

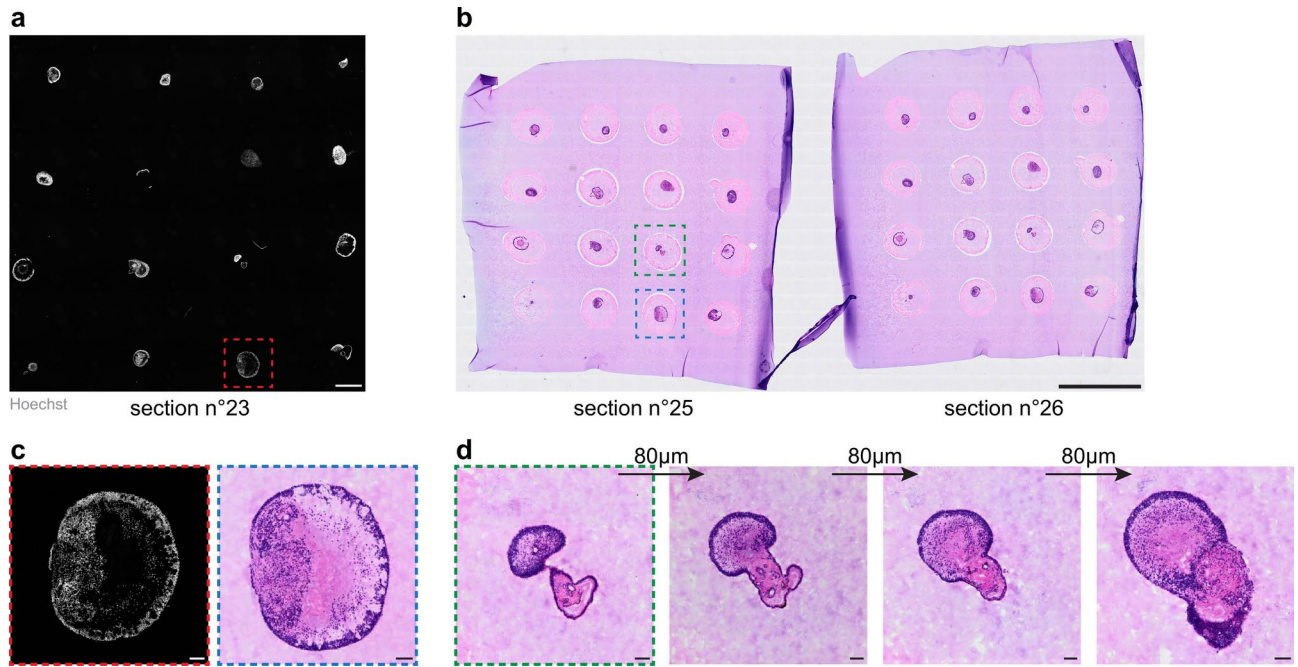


Fig. 5. Enhanced throughput and traceability with HistoBrick. Consecutive cryosections (20 μm sectioning thickness) of HistoBrick showing 16 organoids. All organoids are 33 weeks old. Sections stained with (a) Hoechst (scale bar: 1 mm) and (b) H&E (scale bar: 5 mm). (c) Zoom of one retinal organoid from section n°23, highlighted with red dashed line in (a), and n°25, highlighted with blue dashed line in (b), showing the correlation between Hoechst and H&E staining (scale bars: 100 μm). (d) Consecutive cryosections of one H&E stained organoid from section n°25, highlighted with green dashed line in (b), revealing some aspects of retinal organoid 3D organization (scale bars: 100 μm).

Structural changes of human retinal organoids over time

Retinal organoids require over six months of development to reach a stage where they exhibit transcriptomic and morphological characteristics closely resembling those of the adult human retina¹⁸. We have previously shown that at week 46, the transcriptome of rod photoreceptors changes and some rod marker genes are down-regulated²². It was not known whether from that age onward, organoids would lose photoreceptors, and until when photoreceptors can be maintained in retinal organoids. We cultured retinal organoids for 98 weeks, fixed organoids at week 30, 38, 46, 52, 70, 81 and 98 ($n = 3\text{--}8$ retinal organoids per time-point), and embedded them in PEGDA-gelatine HistoBricks. Processing the organoids using HistoBrick embedding greatly reduced the number of blocks that needed to be sectioned and stained (3 HistoBricks instead of 11 conventional blocks). We then assessed several quality criteria that are potentially compromised in aging organoids: 1. the presence of layered retina structures, 2. the presence of rod- and cone photoreceptors and 3. the presence of photoreceptor outer segments.

We observed organoids that maintained both their outer nuclear layer and inner nuclear layer up to week 98 (Fig. 6a). Staining for the rod marker rhodopsin (RHO) and cone marker arrestin 3 (ARR3) revealed the presence and maintenance of both photoreceptor types up to week 98 in culture. However, while organoids are surrounded by dense outer segments between weeks 30 and 52, we observed a gradual loss of photoreceptor outer segments past week 52 (Fig. 6b). To quantify whether outer segments decrease over time, we estimated the OS + IS thickness ϑ . For each individual organoid, we manually selected the section with the most abundant outer segments for quantification. Our measurements revealed that OS + IS thickness ϑ negatively correlates with time (Fig. 6c, Spearman rank correlation $r = -0.38$, $P = 0.01$). Up to week 52, OS + IS thickness ϑ was significantly larger than the negative control (Fig. 6d). At week 98, we measured a significant decrease of OS + IS thickness ϑ as compared to the positive control (Fig. 6d). Although retina structures and photoreceptors could still be detected, some degeneration events very likely occurred during the long culture period.

While analyzing the stained images, in older organoids we unexpectedly observed displaced nuclei outside the outer nuclear layer, in the area where outer segments are located (Fig. 6b, Supplementary Fig. 5). To determine the cell type identity of these displaced cells, we performed further stainings. The most common cell types for retinal organoids were examined using the markers SOX9 for Müller cell nuclei, MiTF for retinal pigment epithelium cells, and MAP2 for neuronal cells. The displaced cells were negative for Sox9 and MiTF (Supplementary Fig. 5a). The nuclei of the displaced cells in the Hoechst staining overlapped with the stained cell bodies in the MAP2 stained images (Supplementary Fig. 5b–h, left), confirming a neuronal cell identity. Further evaluation of the ARR3 stained images indicated that these cells were cones, (Supplementary Fig. 5b–h, right). Gartner et al. and Lai et al. described displaced nuclei in the region of outer segments in human retinas upon aging^{28,29}. We found examples of displaced cells in both young and old organoids. However, while the displaced

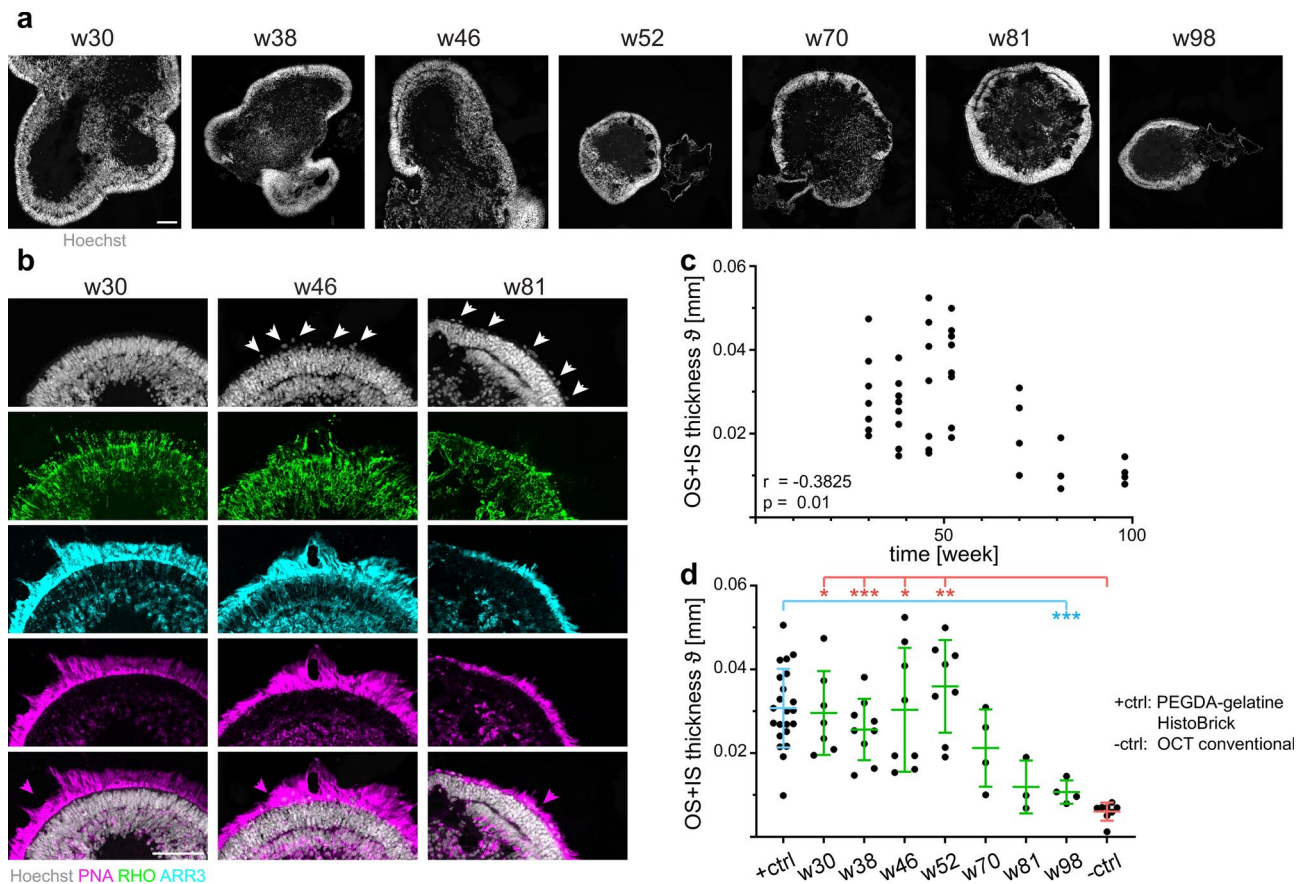


Fig. 6. Structural changes in human retinal organoids upon long-term cultivation for up to 98 weeks. **(a)** Hoechst stained images of embedded organoids of different ages using PEGDA-gelatin HistoBrick embedding, images are of one Z plane. The sections are 25 μm thick (scale bar: 100 μm). **(b)** Immunohistochemistry stained images of three exemplary organoids of different ages (week 30, 46 and 81) with focus on their retinal layer parts to validate outer segment changes over time (scale bar: 100 μm), images are maximum Z projections of Z stacks. The pink arrowheads point to the outer segments, while the white ones point to the displaced nuclei. The sections are 25 μm thick **(c)** Quantification of the change of the OS + IS thickness ϑ of human retinal organoids over time ($n = 3\text{--}4$ organoids from 2 independent differentiation experiments for w30, w38, w46, w52; $n = 3\text{--}4$ organoids from 1 differentiation experiment for w70, w81, w98;). Each dot represents one organoid. Spearman rank correlation coefficient r and P value indicated in the graph. **(d)** Quantification of OS + IS thickness ϑ of human retinal organoids over time. Same data analyzed as in **(c)**, in addition positive control data (PEGDA-gelatin HistoBrick from Fig. 4h) and negative control data (OCT conventional from Fig. 4h) were included. Mean \pm SD indicated in green. One-way Welch's ANOVA, P value < 0.001 ; posthoc Dunnett's test comparing all groups against positive and negative control. Significant P values of the comparisons to the controls are shown on the graph. $P \leq 0.05$ (*), $P \leq 0.001$ (**), $P \leq 0.001$ (***)

cells appeared individually in organoids at week 30 and 38, we saw examples of displaced nuclei arranged chain-like near each other in older organoids (Supplementary Fig. 5b–h).

Discussion

In this work, we present a novel embedding matrix PEGDA-gelatin hydrogel to prepare an adapted HistoBrick for organoid cryosectioning. Identifying a novel embedding mixture was key to adapt the HistoBrick for cryosectioning of complex 3D microtissues. The embedding material should meet the following criteria. First, it should provide structural stability of the sections during cryosectioning. Importantly, a coherent interface between the gel well plate and the embedding matrix prevents the loss of valuable samples. Second, the embedding matrix should support and preserve the sample's structural integrity throughout the whole process. A stable interface between the embedding material and the sample is crucial. Third, handling of the HistoBrick should be easy, including gel well plate unmolding from the silicone mold. Finally, the embedding material solution should allow easy transfer of organoids onto the bottom of the gel well plate.

Ferguson et al. presented an embryoid body array providing traceability for six experimental conditions using OCT as an embedding matrix⁹. The major limitation of this technique resides in the use of OCT which is a viscous material difficult to pipette, solidifying only below $-10\text{ }^{\circ}\text{C}$ ³⁰ and not maintaining fragile structures such as outer segments of retinal organoids¹⁸. Gelatine, which provides good stability to soft samples¹⁶, was

used to create an array of six half rodent brains (cm-scale³¹). The study highlights gelatine as a promising candidate for organoid or tissue arrays in the mm-scale like the HistoBrick. However, gelatine presents the disadvantage of needing to be kept above 37 °C to stay liquid. At room temperature, the viscosity of gelatine increases, making pipetting difficult. Consequently, UV-crosslinkable hydrogels with stable viscosity at room temperature are an interesting embedding matrix for the HistoBrick, facilitating gel pipetting and promoting organoid sedimentation inside the HistoBrick wells. PEGDA is a promising UV-curable candidate because it is widely commercially available, well studied in literature and exhibits biocompatibility properties³². A previous study investigated the cryosectioning of a tissue-engineered construct composed of polyethylene glycol hydrogel (PEG) mixed with human mesenchymal stem cells. The untreated PEG-derived hydrogels were incompatible with the cryosectioning process²¹. This behavior is due to the water-rich and polymeric nature of these compounds, which makes them very sensitive to routine tissue histology procedures. The highly ordered tetrahedral structure of water molecules in large ice crystals results in sample brittleness³³. The authors of the study demonstrated that overnight incubation in OCT or 1% Polyvinyl alcohol (PVA) of the tissue-engineered PEG-derived constructs increases the flexibility of the frozen sample facilitating sectioning²¹. In another study, spheroids cultured in alginate and after fixation embedded in OCT were successfully cryosectioned¹⁴. Alginate was not considered for the HistoBrick fabrication because its crosslinking relies on the diffusion of ions which is difficult to implement for large volumes.

Based on these considerations, we compared gelatine and PEGDA as materials for the HistoBrick. As expected, PEGDA HistoBrick cryoblocks were very brittle and shattered during sectioning. On the other hand, gelatine acts as a plasticizer promoting material flexibility and reducing the sections' brittleness. A small amount of gelatine (2.5 wt%) added to the PEGDA hydrogel enables the cutting of entire crack-free and fold-free sections while maintaining the advantage of easy handling low-viscous solution at room temperature and UV-crosslinking. Using a mixture of 8 v% PEGDA and 2.5 wt% gelatine, the user can prepare PEGDA-based cryoblocks without the need for prolonged overnight incubation in OCT or PVA solution, as required in a related published protocol²¹. Furthermore, the addition of gelatine promotes the adhesion between the gel well plate and the embedding matrix, which is crucial to avoid the loss of precious samples. During freezing and sectioning, a separation of the tissue-matrix interface may create damage to the tissue. Proper infiltration of the embedding matrix inside the tissue promotes a coherent interface. Analysis of the substructure of human retinal organoids revealed that PEGDA-gelatine mixture preserves the fragile structure of outer segments, as well as the organization of the organoid nuclear layers and cell types. It correlates with the stable interface obtained between the embedding matrix and the organoids. Additionally, the PEGDA-gelatine mixture has a 3.4 times lower viscosity at 37 °C than gelatine 7.5 wt%, which promotes the diffusion of the matrix during incubation supporting the structure of fragile tissue¹⁶ (Supplementary Fig. 1b,c).

Embedding with the gelatine HistoBrick protocol frequently resulted in damaged outer segments. The rapid solidification of gelatine during organoid transfer into the well plate required that organoids were pushed into well bottoms with pipette tips (to prevent their attachment to well walls or displacement by air bubbles), which may have damaged the organoids. PEGDA-gelatine circumvented this problem, as it is less viscous at room temperature and thereby more suited for organoid transfer into wells and retained the substructure of retinal organoid outer segments more efficiently. PEGDA-gelatine is thus the preferred material for fabrication and use of a HistoBrick for cryosectioning.

The PEGDA-gelatine HistoBricks easily allowed the analysis of a two-year retinal organoid culture time-course. Instead of preparing and sectioning 11 conventional blocks with different time points and biological replicates, only 3 PEGDA-gelatine HistoBricks were required to analyze all samples. We have previously analyzed the development of retinal organoids in detail by single-cell RNA sequencing and compared them to the adult human retina²². At week 46, we have found the cell type diversity of organoids to be decreased and that some cell type marker genes such as rhodopsin were downregulated in rods²². One could interpret reduced expression of cell type marker genes as a decrease in cell quality or health. The decrease of outer segments that we visually observed from week 52 supports the indication that photoreceptors degenerate to some degree. In some retinal diseases, outer segments of photoreceptors degenerate, while their cell bodies remain viable³⁴. It has been unclear for how long photoreceptors can be maintained in cultured retinal organoids. We were surprised to still find organoids with clearly separated outer nuclear and inner nuclear layers between week 70 and up to week 98. We observed both cone and rod photoreceptors up to week 98.

Unexpectedly, in older organoids we found displaced nuclei that we identified as cones, on top of the outer nuclear layer, in the region where outer segments are. It has been described in sections of human retinas that photoreceptor cell bodies can be displaced out of the outer nuclear layer into the region of outer segments during aging^{28,29}. Further studies are needed to validate whether the gradual loss of photoreceptor outer segments and displacement of cones is a form of degradation in retinal organoids and whether this is similar to degeneration processes happening in human disease or aging.

The HistoBrick method faces general challenges associated with the analysis of complex 3D microtissues on two-dimensional sections. First, each section contains only part of an organoid at a random sectioning angle which may or may not contain the tissue region or cell type of interest (Supplementary Fig. 4c), introducing variability in tissue composition. Second, organoids largely vary in size and shape²⁷, and on each given section only a fraction of the entire organoid is visible, introducing variability in size and geometry. Third, retinal organoids contain not only retina, but also regions of non-retinal identity, introducing variability in the ratio of retinal to non-retinal tissues. Fourth, depending on the cutting angle, appearance of retinal organoid layering, outer segment thickness, or distance between layers could be influenced by the sectioning angle. These sources of variability could be reduced by analyzing a larger number of sections per organoid, or optimally their full 3D signals. In addition, the analysis would benefit from automated organoid segmentation based on antibody staining. A future version of the HistoBrick, potentially using yet another material, could be adapted

to organoid embedding for wholemount staining, clearing and imaging in 3D. Some aspects of the HistoBrick method can be further optimized to improve its user-friendliness. First, color can be added to the embedding material to help the visualization on the slide after sectioning and staining. Secondly, a marking sign visible on transparent sections could be incorporated into the HistoBrick design to ensure optimal sample traceability and re-orientation. Finally, automated transfer of organoids into the gel well plate and automated staining would further increase the throughput of the HistoBrick approach.

We successfully adapted the HistoBrick methodology for an efficient preparation and analysis of organoid frozen sections. We expect the PEGDA-gelatine HistoBrick to provide optimal support to various fragile samples like brain organoids and cochlea biopsies. The PEGDA-gelatine HistoBrick increases the throughput of immunohistochemistry by simultaneously embedding up to 16 human retinal organoids from different experimental conditions in an organized manner. Processing a smaller number of cryoblocks for sectioning and stainings saves time and consumables such as antibodies required for staining the resulting sections (Supplementary Fig. 4d). Depending on the microtissue to analyze, the HistoBrick can easily be adapted to different organoid and tissue sizes, and organoid numbers per block can still be increased when smaller or more wells are used. Simultaneous immunohistochemical staining and imaging of multiple organoid samples on the same section reduces sample-to-sample variation and enables more reliable analysis. The array organization facilitates traceability of individual organoids through different sections and offers high potential for automated organoid transfer and image analysis. Furthermore, the HistoBrick is a versatile labware that can be easily implemented in standard laboratories thanks to its simple methodology and low-cost materials. The ease of HistoBrick re-design enables adoption of the technology across the field of microtissue research. Finally, with this tool in hand, the immunohistochemical validation of organoid high-throughput experiments such as compound-, toxicology-, or gene-therapy screening will be simplified.

Methods

Gel well plate fabrication

The silicone mold was designed similarly to our previous work⁸. The diameter of the wells was increased to 2.4 mm to accommodate large retinal organoids. The outer dimensions of the HistoBrick were set to 20.7×34.7 mm to contain 16 wells (Supplementary Fig. 1a). The mold was 3D printed in silicone “TrueSil Shore 50A” by the company Spectoplast. The schematic of the HistoBrick fabrication is depicted in Fig. 2. The HistoBrick 3D design file is available upon request to the corresponding authors. HistoBrick well-sizes and dimensions can be optimized for different organoid types.

Gelatine gel well plate

In a first approach, the silicone mold was placed with the pillars facing downward on a petri dish. A gelatine solution (7.5 wt% gelatine (Sigma Aldrich, #G1890), 10 wt% sucrose (Sigma Aldrich, #84,100) in 1×PBS) was warmed at 37 °C and pipetted inside the silicone mold. The gelatine solution was crosslinked at 4 °C for 1 h. Afterwards, the mold was flipped and the gel well plate was released by gently lifting it from below. The obtained gel well plate was stored in a closed box with damp paper at 4 °C until use.

PEGDA-based gel well plate

In a second approach the silicone mold was placed with the pillars facing downward on a petri dish. The PEGDA-gelatine solution was prepared by mixing 8 v% PEGDA (Mw = 700, Sigma Aldrich, #455008), 2.5 wt% gelatine (Sigma Aldrich, #G1890), 10 wt% sucrose (Sigma Aldrich, #84100) and 0.05 wt% LAP (Sigma Aldrich, #900889) in 1×PBS. The solution was pipetted inside the silicone mold and crosslinked by a 30 s exposure to 365 nm wavelength light with 35 mW/cm power (total illumination dose = 1.05 J/s*cm). The UV light was shined from above the mold. Afterward, the silicone mold was vertically lifted to release the gel well plate. The obtained gel well plate was stored in a closed box with humid paper at 4 °C until use. For the material selection, additional HistoBricks were prepared using a solution of 8 v% PEGDA Mw = 700, 10 wt% sucrose, 0.05 wt% LAP in 1×PBS and 10 v% PEGDA Mw = 700, 10 wt% sucrose, 0.05 wt% LAP in 1×PBS with the same crosslinking procedure.

Organoid transfer into the gel well plate and HistoBrick freezing

When the gelatine embedding material was used, the gel well plate was left to equilibrate at room temperature for 1 h. We refer to the liquid hydrogel solution filling the wells of the gel well plate as liquid embedding matrix. Before organoid transfer into the gel well plate, PFA-fixed, sucrose-cryopreserved retinal organoids were incubated in liquid embedding matrix of the same embedding material as the gel well plate for 15 min at 37 °C on a warming plate to enhance organoid-embedding matrix interaction. Incubation can also be performed in an incubator at 37 °C. The organoids were manually transferred with 20–50 µL of liquid embedding matrix to the gel well plate with a 200 µL tip pre-coated with 2% BSA (Sigma Aldrich, #A2153) in deionized water, to prevent organoids from sticking. The end of the tip was cut with a razor blade to create a larger aperture to avoid damaging the organoids. The gel well plate can be pre-wet by adding 20 µL of PBS in each well to minimize air bubble trapping. After the transfer, the wells were filled up with the same liquid embedding matrix used during the incubation of the organoids. Organoids were aligned onto a unique plane by centrifuging the filled gel well plate for 20 s at 200×g. The filled gel well plate underwent a second crosslinking (as previously described) to fix the position of the organoids at the bottom of the wells. The HistoBrick blocks were trimmed on all four sides so that three sections would later fit on the glass slides during cryosectioning. Finally, the HistoBrick was fixed on a labelled cardboard with a drop of OCT and snap frozen for 2 min by submersion in isopentane (Sigma Aldrich, #277258) cooled down to – 40 °C using dry ice pellets. The frozen HistoBricks were wrapped in aluminum foil to avoid drying and stored at – 80 °C until cryosectioning.

Conventional cryoblock preparation

Unless specified otherwise, the steps were performed using the same solutions and timings as for the gel well plate fabrication and organoid transfer.

Gelatine and PEGDA-gelatine cryoblock

The respective solution was pipetted inside a plastic weighing boat or an embedding mold and crosslinked to form a base layer of 2–4 mm thickness. During this time, retinal organoids were incubated in their respective embedding solutions for 15 min at 37 °C. Then, they were transferred one by one and placed on the base layer, followed by a second crosslinking. Finally, liquid embedding material was pipetted on top of the organoids to fill up the weighing boat and crosslinked. The blocks were trimmed with a scalpel to leave 1–2 mm space between the organoids and the block edge. The samples were then fixed on a labelled cardboard with a drop of OCT, snap frozen in isopentane at – 40 °C and stored at – 80 °C.

OCT-based cryoblock

OCT (Sakura, #4583) was poured inside a plastic weigh boat and crosslinked by freezing on dry ice pellets to form a base layer. The organoids were then transferred from their storage solution (without incubation) and placed on the base layer. Additional OCT was poured on the organoids, the blocks were frozen on dry ice and stored wrapped in aluminum foil at – 80 °C.

HistoBrick cryoblock and conventional cryoblock sectioning

The HistoBrick cryoblocks and the conventionally embedded cryoblocks were stored at – 20 °C overnight to acclimate to sectioning temperature. They were then mounted on a cryostat holder with OCT. If necessary, HistoBrick cryoblocks were again trimmed to fit 3 sections per slide, and conventional cryoblocks were trimmed to fit 8–12 sections per slide. Then they were sectioned in thin slices of 20 µm or 25 µm and placed on SuperFrost/Plus glass slides (Biosystems, #85-0911-00 or Eprelia, #K5800AMNZ72). For results shown in Figs. 4, 6, Supplementary Figs. 2, 3 and 5 consecutive HistoBrick sections were placed one section per glass slide on 5 slides. Afterwards, a second section was placed on each of the slides, followed by a third section, again starting from the first slide. After filling the first 5 slides, a second slide series of 5 slides was prepared using the same procedure. In this manner each slide contains sections from different organoid cutting depths, increasing the likelihood that there will be at least one usable section per organoid. The slides were stored at – 20 °C or – 80 °C until staining.

Hematoxylin and Eosin staining

To localize the organoids, slides were stained with hematoxylin and eosin. The slides were equilibrated and dried at room temperature for 1 h, then rehydrated in deionized water for 10 min. The slides were then incubated in Harris Hematoxylin (Harris Hematoxylin: Biosystems, #3873.2500) for 5 min and washed with running tap water. They were then differentiated for a few seconds in 1% acid-alcohol (Absolute alcohol: 7:10, VWR #20820.362, Hydrochloric acid 37%: 0.1:10, Sigma Aldrich, #30721 and H₂O MiliQ 2.9:10) and washed under running tap water for 10 min. The slides were incubated in Eosine-Phloxine solution for 1 min (Eosin: 1:100, Sigma Aldrich, #E4382; Phloxine: 1:100, Sigma Aldrich, #P2759) and washed a last time. Finally, the slides were mounted with Eukitt (Sigma Aldrich, #03989) and dried overnight at room temperature.

Immunostainings

The slides were equilibrated and dried at room temperature for 1 h, then rehydrated in 1×PBS for 10 min. The sections were blocked with 180 µL of 10% NDS blocking solution (10% Normal Donkey Serum (Sigma Aldrich, S30-M), 1% BSA (Sigma Aldrich, #A2153), 0.5% TritonX (Sigma Aldrich, #T9284), 0.1% sodium azide (Biosciences, #786-299), 1×PBS) for 1 h. The blocking solution was removed, and the primary antibodies were added (ARR3: 1:400, Sigma Aldrich, #HPA063129; PNA: 1:1200, Sigma Aldrich #L6135; Rhodopsin: 1:400, Sigma Aldrich, #R5403; SOX9: 1:200, R&D systems, #AF3075; MiTF: 1:500, Exalpha, #X2398M; MAP2: 1:400, Sigma Aldrich, #AB5622; OneCut2: 1:100, R&D systems, # AF6294; Cralbp: 1:200, Abcam, #ab15051; Trpm1: 1:200, Sigma Aldrich, #HPA014779; Bassoon: 1:500, Enzo, # SAP7F407, L-M Opsin: 1:100, Merck, # AB5405). The primary antibodies were diluted in a 3% NDS solution (3% Normal Donkey Serum, 1% BSA, 0.5% TritonX, 0.1% sodium azide, 1×PBS), 180 µL was added to each slide. The sections were covered with parafilm and incubated with the primary antibodies overnight at 4 °C in a humidified chamber. Afterwards, the slides were washed 3 times with PBS-T (1×PBS, 0.05% TritonX) for 10 min each. The secondary antibodies (Hoechst 33342: 1:2000, Invitrogen, #H3570; anti-Mouse 488: 1:500, Invitrogen, #A32766; Streptavidin 555: 1:400, Invitrogen, #S32355; anti-Rabbit 640: 1:500, Invitrogen, #A32795; anti-Goat 488: 1:500, Invitrogen, #A32814; anti-Mouse 568: 1:500, Invitrogen, #A10037; anti-Sheep 488: 1:500, Invitrogen, # A11015) were diluted in 3% NDS and the sections were incubated for 2 h with 180 µL antibody solution at 4 °C. The slides were washed twice with PBS-T for 10 min each and once with 1×PBS for 10 min. As a last step, the slides were mounted with Prolong Gold (Invitrogen, #P36934), coverslipped, and dried overnight at room temperature, sealed with nail polish (Electron Microscopy Sciences, #72180) and imaged.

Image acquisition

Images of the H&E-stained sections in Figs. 3 and 5 were acquired with an Olympus VS200 slide scanner. An overview image of the entire glass slide was acquired at 10x (UplaXapo, NA = 0.40) magnification in brightfield. Immunostained sections were acquired with a confocal spinning disc microscope (Olympus IXplore SpinSR10). Different magnifications were used depending on the desired image (4x: UplanSApo, NA = 0.16; 10x: UplanSApo, NA = 0.40; 20x: UplanSApo, NA = 0.75; 40x: UplanSApo, NA = 1.05 Sil). For higher throughput of image

acquisition and in Supplementary Fig. 3, a slide scanner was used (Zeiss Axio Scan.Z1) with 10× magnification (Plan-Apochromate, NA=0.45). OS+IS area measurements were performed on images obtained with the Zeiss Axio Scan.Z1 slide scanner. For each individual organoid, the section containing the highest quality outer segments (criteria: abundant OS with as little disruption as possible, intact organoid section) was manually selected for analysis.

Image analysis

Analysis of the vertical alignment of the human retinal organoids was performed on consecutive H&E-stained sections on a slide series by manually counting the number of organoids present on each section. For each HistoBrick, we determined the number of sections in which at least 80% of the organoids were visible. The analysis was conducted on two HistoBricks containing 15, respectively 16, organoids. Although the HistoBrick contains a marking at one edge to localize the top right corner, one well can be left empty for experiments in which the embedding matrix cannot easily be visualized during the microscopy step. This improves the certainty of organoid re-identification, because during sectioning and microscopy the sections and the images thereof can be rotated.

FIJI²⁶ was employed in this study for image modification and the quantification of the OS+IS area within images. For images displayed in the figures, brightness and contrast were adjusted for optimal visualization of the signal. Each channel underwent independent analysis.

OS + IS area measurements

To obtain single, fully filled regions of interest (ROIs), we applied the following procedure separately for each channel. For area masking, first, the “Fire” lookup table (LUT) for color mapping was applied to enhance visualization (Supplementary Fig. 3c, 2nd panel). A color threshold was manually set for each channel such that the organoid including the OS was above, and the background below threshold. Thresholds were channel-specific and kept constant within one embedding material in Fig. 4 and across all conditions in Fig. 6. A binary mask was defined as the pixels above threshold (Supplementary Fig. 3c, 3rd panel).

Image parts of the retinal organoids below threshold were included into the mask (Supplementary Fig. 3d), while parts outside the retinal organoid with values above threshold, including non-retinal, unstructured or disrupted organoid regions were manually separated from the mask (Supplementary Fig. 3e) using the “Overlay brush” tool. Subsequently, the “Fill Holes” command was executed to include all pixels inside the retinal organoid into the mask. The “Analyze Particles” function was applied to define a region of interest (ROI) by the binary mask with the largest area, corresponding to the retinal organoid (Supplementary Fig. 3c, right panel, Supplementary Fig. 3d,e, right panels).

Area measurements of the ROIs were performed using the “Analyze Particles” command. To measure the OS+IS area, first, a single, fully filled ROI for the Peanut agglutinin (PNA) signal was determined (PNA ROI, Supplementary Fig. 3b,c). Second, a single, fully filled ROI for the Hoechst signal was determined (Hoechst ROI, Supplementary Fig. 3b,c). Finally, to calculate the OS+IS area, the area of the Hoechst ROI was subtracted from the area of the PNA ROI.

The used FIJI macro is available in the Supplementary Information.

Quantification of OS + IS thickness

To quantify outer segments independent of organoid size and cross-section area, we estimated the average thickness ϑ of the outer and inner segments labeled by PNA (“OS+IS thickness”) by

$$\vartheta = \frac{\sqrt{PNAarea}}{\sqrt{\pi}} - \frac{\sqrt{Hoechstarea}}{\sqrt{\pi}}$$

where PNA area denotes the area of the PNA ROI and Hoechst area denotes the area of the Hoechst ROI. ϑ provides the exact solution for circular organoids with uniform OS+IS segments and an average thickness estimate for organoids with less regular shape and OS+IS segments. ϑ can also be expressed as a ratio between the OS+IS area and the Hoechst area, providing an intuitive interpretation of their relationship:

$$\frac{OS + ISarea}{\sqrt{Hoechstarea} \cdot \sqrt{\pi} \cdot 2} = \frac{PNAarea - Hoechstarea}{\sqrt{Hoechstarea} \cdot \sqrt{\pi} \cdot 2} = \frac{(2 \cdot r \cdot \vartheta + \vartheta^2) \cdot \pi}{r \cdot \sqrt{\pi} \cdot \sqrt{\pi} \cdot 2} = \vartheta + \frac{\vartheta^2}{2r} \approx \vartheta,$$

with radius r of the Hoechst area, radius $r + \vartheta$ of the PNA area, and $\vartheta \ll r$.

Retinal organoid culture and fixation for embedding

Retinal organoids were generated from induced pluripotent stem cells as previously described in Cowan et al. and Spirig et al.^{22,27}. Retinal organoids were generated from the induced pluripotent stem cell line 01F49i-N-B7 (IOBi001-A (RRID:CVCL_C1TR) described in Cowan et al.²². Experiments in this study were performed using organoids aged between 30 and 98 weeks. Organoids were fixed using 4% paraformaldehyde (PFA) (Merck, #1.00496) for 4 h at 4 °C. The samples were washed three times for 10 min each in 1×PBS. Then the organoids were incubated in 30% sucrose (Millipore, #84100) in 1×PBS until sunken to the bottom of the tube for cryopreservation and stored at − 80 °C until embedding.

Statistical analysis

Graphpad Prism (Prism10 for MacOS, Version 10.3.1 (464), August 21, 2024) was used for statistical analysis. To test whether the OS + IS thickness ϑ labeled by PNA differed significantly for the results shown in Figs. 4h and 6d, Welch's ANOVA was used to compare the different groups followed by posthoc Dunnett's test. For the posthoc test in Fig. 4h, we compared all conditions to the conventional gelatine embedding. For the graph in Fig. 6d, we included data from Fig. 4 as controls. We used the PEGDA-gelatine HistoBrick data as positive controls and the OCT data as negative controls. For the posthoc test, we compared all against negative control and all against positive control.

To determine, whether OS + IS thickness ϑ decreases over time, we plotted ϑ values of the organoids at different developmental ages against their age in weeks. We then calculated the nonparametric Spearman rank correlation. The P value and r are represented in the figure.

Multiplicity adjusted P values are indicated as asterisks in the figures as follows: $P > 0.05$ (ns), $P \leq 0.05$ (*), $P \leq 0.001$ (**), $P \leq 0.001$ (***). Only significant P values were indicated on the graphs, the other comparisons were not significant. Each dot on the graphs represents the results of one organoid.

Rheological measurements

The gelatine solution, PEGDA-gelatine solution and a 8 v% PEGDA + 10 wt% sucrose solution were measured by pipetting 1 ml of the solution into a rheometer (Anton Paar, MCR 702e). For oscillation testing, the geometry used was a PP-40 with a gap of 0.5 mm. The normal force was set at 0 N so that the gap would adjust to maintain this force during the phase transition. A ramp from 37 to 20 °C (5 °C/min) followed by an isotherm at 20 °C for 60 min was performed for the gelatine solution and the PEGDA-gelatine solution. For the PEGDA solution, a ramp from 37 to 20 °C (5 °C/min) followed by an isotherm at 20 °C for 10 min was performed. The isotherm at 20 °C was shortened for the PEGDA solution because it showed stable behavior. During these 2 intervals, the storage Modulus (G') and the loss Modulus (G'') as well as the complex viscosity were recorded at a strain of 1% and 1 Hz. Prior to this experiment, an amplitude sweep test was performed (data not shown) to evaluate the Linear viscoelastic range (LVE range). 1% strain was selected within the LVE range. For rotational testing, the geometry used was a CP-50-1 (diameter of 50 mm with a 1° angle and cone truncation of 0.045 mm). Dynamic viscosity was recorded at 37 °C from a shear rate of 0.1–1000 s⁻¹. The exploitable data range is from 10 to 1000 s⁻¹. The rotational tests were performed three times for each sample. The dynamic viscosities of the different solutions were calculated as the average of the three performed tests over the whole shear rate range.

Data availability

The datasets generated and analyzed during the current study are available from the corresponding authors on reasonable request.

Received: 11 July 2024; Accepted: 11 December 2024

Published online: 02 January 2025

References

- Hira, V. V. V. et al. Comparison of different methodologies and cryostat versus paraffin sections for chromogenic immunohistochemistry. *Acta Histochem.* **121**, 125–134 (2019).
- Zupančič, D., Terčelj, M., Štrus, B. & Veranič, P. How to obtain good morphology and antigen detection in the same tissue section?. *Protoplasma* **254**, 1931–1939 (2017).
- Clevers, H. Modeling development and disease with organoids. *Cell* **165**, 1586–1597 (2016).
- Kim, J., Koo, B.-K. & Knoblich, J. A. Human organoids: model systems for human biology and medicine. *Nat. Rev. Mol. Cell Biol.* **21**, 571–584 (2020).
- Vuille-dit-Bille, E. et al. Tools for manipulation and positioning of microtissues. *Lab. Chip* **22**, 4043–4066 (2022).
- Lukonin, I., Zinner, M. & Liberali, P. Organoids in image-based phenotypic chemical screens. *Exp. Mol. Med.* **53**, 1495–1502 (2021).
- Spirig, S. E. & Renner, M. Toward retinal organoids in high-throughput. *Cold Spring Harb. Perspect. Med.* **14**, a041275 (2024).
- Heub, S. et al. Coplanar embedding of multiple 3D cell models in hydrogel towards high-throughput micro-histology. *Sci. Rep.* **12**, 9991 (2022).
- Ferguson, R. & Subramanian, V. Embryoid body arrays: Parallel cryosectioning of spheroid/embryoid body samples for medium through-put analysis. *Stem Cell Res.* **28**, 125–130 (2018).
- Ivanov, D. P. & Grabowska, A. M. Spheroid arrays for high-throughput single-cell analysis of spatial patterns and biomarker expression in 3D. *Sci. Rep.* **7**, 41160 (2017).
- Moraes, G. D. S., Wink, M. R., Klamt, F., Silva, A. O. & Da Cruz Fernandes, M. Simplified low-cost methodology to establish, histologically process and analyze three-dimensional cancer cell spheroid arrays. *Eur. J. Cell Biol.* **99**, 151095 (2020).
- Gabriel, J., Brennan, D., Elisseff, J. H. & Beachley, V. Microarray embedding/sectioning for parallel analysis of 3D cell spheroids. *Sci. Rep.* **9**, 16287 (2019).
- Sabaliauskas, N. A. et al. High-throughput zebrafish histology. *Methods* **39**, 246–254 (2006).
- Kang, J. et al. Mini-pillar array for hydrogel-supported 3D culture and high-content histologic analysis of human tumor spheroids. *Lab. Chip* **16**, 2265–2276 (2016).
- Zhang, S.-W. et al. An efficient and user-friendly method for cytohistological analysis of organoids. *J. Tissue Eng. Regen. Med.* **15**, 1012–1022 (2021).
- Nagamoto-Combs, K., Manocha, G. D., Puig, K. & Combs, C. K. An improved approach to align and embed multiple brain samples in a gelatin-based matrix for simultaneous histological processing. *J. Neurosci. Methods* **261**, 155–160 (2016).
- Hurley, P. A., Clarke, M., Crook, J. M., Wise, A. K. & Shepherd, R. K. Cochlear immunochemistry—a new technique based on gelatin embedding. *J. Neurosci. Methods* **129**, 81–86 (2003).
- Berber, P., Bondarenko, S., Michaelis, L. & Weber, B. H. F. Transient retention of photoreceptor outer segments in matrigel-embedded retinal organoids. *Int. J. Mol. Sci.* **23**, 14893 (2022).
- Brown, D. A., Chou, Y. F., Beygui, R. E., Dunn, J. C. Y. & Wu, B. M. Gelatin-embedded cell-polymer constructs for histological cryosectioning. *J. Biomed. Mater. Res. B Appl. Biomater.* **72**, 79–85 (2005).

20. Griffioen, H. A., Van der Beek, E. & Boer, G. J. Gelatin embedding to preserve lesion-damaged hypothalami and intracerebroventricular grafts for vibratome slicing and immunocytochemistry. *J. Neurosci. Methods* **43**, 43–47 (1992).
21. Ruan, J.-L. et al. An improved cryosection method for polyethylene glycol hydrogels used in tissue engineering. *Tissue Eng. Part C Methods* **19**, 794–801 (2013).
22. Cowan, C. S. et al. Cell types of the human retina and its organoids at single-cell resolution. *Cell* **182**, 1623–1640.e34 (2020).
23. Afanasyeva, T. A. V. et al. A look into retinal organoids: methods, analytical techniques, and applications. *Cell. Mol. Life Sci.* **78**, 6505–6532 (2021).
24. Rosa, J. G. S., Disner, G. R., Pinto, F. J., Lima, C. & Lopes-Ferreira, M. Revisiting retinal degeneration hallmarks: Insights from molecular markers and therapy perspectives. *Int. J. Mol. Sci.* **24**, 13079 (2023).
25. Ferrari, S. et al. Retinitis pigmentosa: genes and disease mechanisms. *Curr. Genom.* **12**, 238–249 (2011).
26. Schindelin, J. et al. Fiji: an open-source platform for biological-image analysis. *Nat. Methods* **9**, 676–682 (2012).
27. Spirig, S. E. et al. Cell type-focused compound screen in human organoids reveals CK1 and MAPK11 inhibition protects cone photoreceptors from death. Preprint at <https://doi.org/10.1101/2023.10.09.561525> (2024)
28. Lai, Y.-L. et al. Subretinal displacement of photoreceptor nuclei in human retina. *Exp. Eye Res.* **34**, 219–228 (1982).
29. Gartner, S. & Henkind, P. Aging and degeneration of the human macula. 1. Outer nuclear layer and photoreceptors. *Br. J. Ophthalmol.* **65**, 23–28 (1981).
30. Tissue-Tek O.C.T. Compound | O.C.T. Compound | Sakura Finetek USA. <https://www.sakuraus.com/Products/Cryotomy/Tissue-Tek%20ae-O-C-T-Compound.html>.
31. Stæger, F. F. et al. A three-dimensional, population-based average of the C57BL/6 mouse brain from DAPI-stained coronal slices. *Sci. Data* **7**, 235 (2020).
32. Choi, J. R., Yong, K. W., Choi, J. Y. & Cowie, A. C. Recent advances in photo-crosslinkable hydrogels for biomedical applications. *BioTechniques* **66**, 40–53 (2019).
33. Yang, C.-C., Jenkins, L. & Burg, K. J. L. Adapted cryosectioning method for hydrogels used in regenerative medicine. *J. Histotechnol.* **30**, 185–191 (2007).
34. Sahel, J.-A. et al. Functional rescue of cone photoreceptors in retinitis pigmentosa. *Graefes Arch. Clin. Exp. Ophthalmol.* **251**, 1669–1677 (2013).

Acknowledgements

The authors thank the Imaging Core Facility (IMCF, Biozentrum, University of Basel). In particular, we thank Sheida Hadji Rasouliha for her technical assistance provided with the Zeiss Axio Scan.Z1 Slide scanner and Sébastien Herbert for his help with our segmentation quantification analysis. We thank R. Wimbish and E. Kastanaki, for comments on the manuscript. We thank Z. Raics for quantifying organoid sizes. The authors thank Jessica Sordet-Dessimoz and her team at the Histology Core Facility at EPFL for the processing of samples for histology. The schematic illustrations were drawn using Biorender Software (Created with BioRender.com). This research was supported by the Swiss Innovation Agency under the Innosuisse Project 57515.1 IP-LS.

Author contributions

E.V.-D.-B. tested the different hydrogel formulations for the HistoBrick preparation and cryosectioning and established protocols for the HistoBrick embedding under supervision of S.H. E.V.-D.-B. performed the rheological tests. E.V.-D.-B. prepared, sectioned, imaged, and analyzed the samples for the alignment study. E.V.-D.-B., D. L.-P. and L.U prepared the samples for the study on structural integrity of organoids. L.U. sectioned, stained, imaged the samples for the study on structural integrity of organoids. L.U., F.E.M. and S.E.S. developed the method for outer segment analysis. L.U., F.E.M. and M.R. analyzed the samples for the study on structural integrity of organoids. L.U. prepared, sectioned, stained and imaged the samples for the time-course study. L.U., F.E.M. and M.R analyzed the samples for the time-course study. V.A.M., Y. H. and L.U. cultured the human retinal organoids under supervision of M.R. S.E.S. measured the organoid population size. E.V.-D.-B., L.U., F.E.M., S.H. and M.R. interpreted data and wrote the manuscript. S.E.S., G.W., D.L.-P., J.G. evaluated the data and all authors reviewed the manuscript.

Declarations

Competing interests

The authors declare no competing interests.

Ethical approval

The work with human induced pluripotent stem cells was approved by the local ethics commission, Ethikkommission Nordwest- und Zentralschweiz EKNZ. All experiments were performed in accordance with local guidelines and regulations. The donor from which the induced pluripotent stem cells were reprogrammed gave informed consent.

Additional information

Supplementary Information The online version contains supplementary material available at <https://doi.org/10.1038/s41598-024-83164-2>.

Correspondence and requests for materials should be addressed to E.V.-d.-B. or M.R.

Reprints and permissions information is available at www.nature.com/reprints.

Publisher's note Springer Nature remains neutral with regard to jurisdictional claims in published maps and institutional affiliations.

Open Access This article is licensed under a Creative Commons Attribution-NonCommercial-NoDerivatives 4.0 International License, which permits any non-commercial use, sharing, distribution and reproduction in any medium or format, as long as you give appropriate credit to the original author(s) and the source, provide a link to the Creative Commons licence, and indicate if you modified the licensed material. You do not have permission under this licence to share adapted material derived from this article or parts of it. The images or other third party material in this article are included in the article's Creative Commons licence, unless indicated otherwise in a credit line to the material. If material is not included in the article's Creative Commons licence and your intended use is not permitted by statutory regulation or exceeds the permitted use, you will need to obtain permission directly from the copyright holder. To view a copy of this licence, visit <http://creativecommons.org/licenses/by-nc-nd/4.0/>.

© The Author(s) 2024